International Journal of Adhesion & Adhesives 118 (2022) 103230

Contents lists available at ScienceDirect

International Journal of Adhesion and Adhesives

journal homepage: www.elsevier.com/locate/ijadhadh

Estimating microscale DE parameters of brittle adhesive joints using genetic expression programming

Xing-er Wang [a,c,d], Armin Yousefi Kanani [a,b], Zewen Gu [a], Jian Yang [c,d,e], Jianqiao Ye [a], Xiaonan Hou [a,*]

[a] Department of Engineering, Lancaster University, Lancaster, LA1 4YW, UK
[b] Mechanical Engineering Group, School of Engineering, University of Kent, Canterbury, CT2 7NL, UK
[c] State Key Laboratory of Ocean Engineering, Shanghai Jiao Tong University, Shanghai, 200240, PR China
[d] Shanghai Key Laboratory for Digital Maintenance of Buildings and Infrastructure, School of Naval Architecture, Ocean and Civil Engineering, Shanghai Jiao Tong University, Shanghai, 200240, PR China
[e] School of Civil Engineering, University of Birmingham, Birmingham, B15 2TT, UK

ARTICLE INFO

Keywords:
Adhesive joint
Discrete element method
Genetic algorithm
Composite materials
Adhesive

ABSTRACT

Particle-based model has strength and flexibility in modelling the microstructures of adhesives and interface in adhesive joints. In this work, a procedure with genetic expression programming (GEP) technique to calibrate the microscale parameters of discrete element (DE) model was proposed for brittle adhesives. Two categories of adhesive properties, the bulk property of thick adhesive and interlaminar-like property of thin adhesive, were discussed. For the bulk property, three target properties of adhesives, i.e. tensile strength, peak strain, secant modulus, were set as the reproduced features. 300 sets of adjustable microscale parameters were produced to run the numerical tests and generate datasets. GEP was then employed to find regression formulas for predicting the target properties as a function of the microscale parameters. For the interlaminar-like property, fracture energies of the cohesive failure of thin adhesives were approximated. A similar procedure of combined DE modelling and GEP was performed to find the regression models to estimate the fracture energy. The developed regression formulas can cover a general range of brittle adhesives. Loctite EA 9497 adhesive was selected to perform a series of lab tests, of which the results were subsequently used to examine the applicability of the DE model with calibrated parameters. The numerical results exhibit good agreements with testing data and observation.

1. Introduction

In recent decades, the applications of adhesive joints can see a significant rise in manufacturing load bearing components, as they have strengths such as lightweight, better fatigue resistance, ability to bond different materials or making composites [1–3]. This requires reliable design models that can suit different configurations of joints and selections of adhesives, which are on the basis of understanding the mechanical performance and failure mechanism of the joints.

Many reports concerning the laboratory works, which are commonly conducted as the first step to observe the actual performance of joints, can be found [4]. Wagih et al. [5] experimentally tested a novel adhesive joint, of which the concept was bio-inspired to optimize the bond line design. Boutar [6] investigated the fatigue resistance of polyurethane (PU) adhesive joint used in automotive manufacturing. Two vital design parameters, adhesive thickness and roughness, were considered to find their optimum combination. Tan et al. [7] experimentally examined the fatigue behaviour of PU adhesive joint under the influences of service temperature. The results indicate that low temperature may easily yield the interfacial failure whilst the cohesive failure is more frequently seen with high temperature case. Popular adherends such as glass, stainless steel, timber, aluminium and various composites can be frequently seen in current experimental reports [8–11], as the selection of adherends will result in various failure modes. It is also found that the adhesive thickness yields significant influences on the fracture toughness of joints [12] as it leads to a variation of plastic zone or fracture process zone (FPZ) at the crack tip.

In addition to the experimental approaches, in order to capture more insightful information of the failure mechanism of adhesive joints, numerical methods have been widely employed [13,14]. The adhesive in

* Corresponding author.
E-mail address: x.hou2@lancaster.ac.uk (X. Hou).

https://doi.org/10.1016/j.ijadhadh.2022.103230
Received 15 March 2022; Received in revised form 4 July 2022; Accepted 19 July 2022
Available online 31 July 2022

the joints is usually a thin layer, which presents an interlaminar-like behaviour once the cracks initiate and propagate [15,16]. Finite element (FE) method might be the most widely used technique in recent years [17]. In order to simulate the interlaminar-like crack propagation, it was combined with several enhanced approaches such as the virtual crack closure technique (VCCT) [18], the cohesive zone models (CZM) derived from the experimental results [19] or the constitutive models based on fracture mechanics or continuum damage laws [20–22]. FE analysis with CZM technique has attracted growing attentions of researchers in recent years as it is more practical and has flexibility in modelling mixed mode failure problem [23]. Many studies using CZM method in adhesive joints can be found [24–26]. Kim et al. [20] conducted a comparative study of the above mentioned four FE techniques in simulating the mixed-mode failure characteristics of adhesive joints with various joint types or configurations. The results show that CZM and continuum damage model (CDM) are most accurate to predict the failure load as a whole. However, the CZM and CDM require the model parameters derived from a series of experiment if different configurations or joint designs are used. For example, the influences due to the adhesive thickness and adherend stiffness on the model parameters cannot be adaptively modelled so far.

In addition, the mechanical performance of adhesive joints presents high sensitivity to different factors in the manufacturing procedure, e.g., surface treatment, curing time of adhesive, manufacturing quality of joints [27,28]. For instance, Akman et al. [29] employed fiber laser to make rough grooves on the adherend surface and proposed an optimized groove design for adhesive joint. It is expected that an appropriate manufacturing procedure can guarantee the robustness of its mechanical performance. However, it is found that adhesive joints may still exhibit a great scatterness of their mechanical performances, even a consistent manufacturing procedure has been adopted [30]. This might be caused by the microstructural features of adhesive joints such as the voids of adhesive, the microscale surface roughness of adherends. However, difficulties rise when using FE technique to consider the microscale features. Instead, discrete element method (DEM) might be more applicable to introduce the complex microstructures [31,32]. The efforts using DEM related to the adhesive joints are extremely limited.

Nevertheless, as well known, the microscopic parameters in DE models demand a calibration procedure to suit different scenarios [33]. The bulk and interlaminar-like properties of adhesives are the key features to predict the actual performance of adhesive joints. Thus, their calibrations should be performed to achieve accurately universal solutions. However, the related works within DEM framework are absent. The characterization of the DE parameters also demands the experience of the researcher, as there might not be straightforward approaches to determine the concerned properties by adjusting so many microscopic parameters [34]. Therefore, the calibration work is usually cumbersome.

Two novelty points are developed in this work: (1) a novel machine learning based approach was developed to find practical symbolic regression models, which can facilitate the estimation on the microscale parameters of adhesives in a more straightforward manner; (2) The bulk property and interlaminar-like property of adhesive, which might be the most significant features in the joint design, can be rapidly calibrated and used to develop a micromechanical model for adhesive joints. The model is able to adaptively capture the mechanical performance of different adhesive joints due to the variation of design variables such as adhesive thickness, without the need to conduct more experiments to derive the associated behaviours.

First, this work introduced a smart algorithm based on genetic expression programming (GEP) method, to develop practical formulas for determining DE parameters for the interested properties of brittle adhesives. For the bulk properties, three target properties, tensile strength, peak strain, secant modulus, were determined to be calibrated. The formulas can then be obtained via GEP based on the datasets from the virtual experiments, in which 300 numerical uniaxial tests of different joint configurations with adjustable microscopic parameters were performed. It was followed by a similar procedure to characterize the interlaminar-like properties, which can achieve satisfactory fracture energies in both normal and tangential directions through the cohesive fractures of adhesives. The calibrated parameters were then validated with those from uniaxial tensile tests, double cantilever beam (DCB) and end notched flexure (ENF) tests. Finally, the model reliability was examined by comparing a micromechanical model which was developed using an example of single lap joint (SLJ) with the testing data.

2. Bulk property of thick adhesives

In certain designs of adhesive joint, thick adhesives might be used to bond or seal the components, for example, the thick structural adhesives used in glass products. The bulk property is then suitable to be adopted in DE model as the thick adhesive is less influenced by boundary constraints. The uniaxial tensile test which was commonly used to obtain bulk property was numerically modelled to generate the datasets for the GEP model in this section.

2.1. Principle of DEM

DEM was originally devised for the problems related to the granular matter which can be characterized by discrete particles [35]. In DEM, it allows for the finite displacement and rotation of particles and is able to automatically track the new contacts or detachments between particles. Particle flow code (PFC) software [36] was adopted to perform the simulation in this work. It uses an explicit and time-marching algorithm to solve the equations. The motion equations are described by the resultants of the force and moment of force between the contacted particles, which can be calculated by Ref. [37]:

$$\text{Linear motion} \quad mi\frac{d^2xi}{dt^2} = mig + \sum_{j=1}^{n} Fij \tag{1}$$

$$\text{Rotational motion} \quad Ii\frac{d\omega i}{dt} = \sum_{j+1}^{n} ri \times fij \tag{2}$$

where t is time, m_i is the particle mass, x_i represents the displacement vector. F_{ij} is the vector of normal contact force, g is the gravitational acceleration, n denotes the number of particles contacted. I_i is the mass moment of inertia, ωi is the vector of angular velocity, r_i is the radius vector of the ith particle, f_{ij} denotes the frictional vector. The subscript i refers to ith particle being contacted, whilst j indicates the jth particle having contact with ith particle.

Contact models with different force-displacement laws can be assigned between neighboring particles to describe the mechanical behaviour of materials [38]. In particular, the bond models which are commonly seen as the distributed elements (e.g., springs, dashpots) at the contact point or surface can be used to connect the discrete bodies. The bonded particles with appropriate bond models and parameters can represent different solid materials. Parallel bond model has been frequently used to model the quasi brittle material [39]. On its basis, soft bond model with allowing for the softening phase of force-displacement law is more suitable for soft materials and hence is used here.

2.2. Virtual uniaxial tensile tests using DEM

Virtual experiment of uniaxial tensile test on adhesive samples was conducted, in which the core testing area of a dumbbell shape adhesive specimen was modelled based on actual experiment. The DE model of the adhesive was then simplified to a random packing of particles with a size of 21 mm × 5 mm. The soft-bond model enabling the varieties of softening stage was employed to connect the particles. In this model, many parameters can be adjusted to generate a wide range of material behaviours, however, this will bring significant difficulties to give a

practical and reliable regression model. Thus, eleven microscopic parameters differing from their default values were used in the standard DE model [36]. Through preliminary trial tests, four parameters were selected to be fixed with constant values (Table 1) whereas seven parameters can be adjusted within a suggested range (Table 2) to achieve the interval of macroscopic material properties.

The fixed parameters in Table 1 are used to adjust the bond behaviour from a parallel bond to a soft bond. For example, when softening factor (sb_soft) is zero, the bond behaviour is essentially same as that of parallel bond. The increase of softening factor indicates a greater ability of softening after peak strength. Softening occurs when the post-peak stress is lower than the product of the peak strength and softening tensile strength factor (sb_cut). It should also be noted that in Table 2, effective modulus represents an overall modulus considering both that of particles and contacts, as soft bond model does not consider a realistic particle stiffness. Radius multiplier (sb_rmul) is used to adjust the influencing radius of generated contacts. Its increase can enhance the further bending and twisting moments. Differing from other solid materials such as rocks or soil which demand the frictional behaviour, the adhesive material is expected to have limited capability to dissipate energy via friction. In addition, only static behaviour is considered in the calibration. Thus, the parameter friction is not treated as one calibrated parameter. Instead, the friction angle which controls the coupling effect between normal and tangential strength of bonds is used.

Three macroscopic properties, i.e. tensile strength, peak strain and secant modulus, were determined to be the targets for validation. The nonlinearity of the material behaviors can be better described by introducing more macroscopic properties, e.g., using more secant modulus at different strain points can promote the fitting of the nonlinear growth and even the ability of strain energy storage. However, this will greatly increase the difficulties to determine the microscopic parameters if more properties are expected to have a perfect solution. In certain cases, the perfect solution does not exist as the involved bond model might have inherent flaws to obtain every realistic property. Thus, only three key properties are used in this work. By adjusting the above-mentioned microscopic parameters within the corresponding range, the target properties of brittle adhesive were found to be within the ranges of 5–112 MPa for tensile strength, 0.0016–0.025 for peak strain, 1.3–41.5 GPa for secant modulus at strain of 0.001. Note that the peak strain here refers to the strain at stress reaching the tensile strength, the tensile strength of bond is set as half of reference strength (sb_ref_str, *fr*).

GEP algorithm requires adequate number of datasets to run the training and validation procedure for obtaining the regression formulas of target properties. The dataset includes both the adjustable microscopic parameters as the input variables and the target property as the predicted output. A fine distribution and combination of input variables as well as the reliable datasets is necessary in the GEP model. Therefore, two steps of preparation were carried out first:

(1) Latin Hypercube Sampling (LHS) method was adopted to generate 300 groups of adjustable microscopic parameters within the defined range. It is worth noting that as the inherent relationships amongst the parameters are not clear or even do not exist, the parameters are assumed to be independent during the sampling.

Table 1
Fixed parameters of standard DE model.

ID	Keyword	Description	Values
1	porosity	Porosity of packing particles	0.1
2	sb_soft	Softening factor	100
3	sb_cut	Softening Tensile strength factor	0.9
4	sb_fa	Friction angle (°)	30

Table 2
Adjustable parameters of standard DE model.

ID	Symbol	Keyword	Description	Range
1	E_m	sb_emod	Effective modulus (MPa)	$(2 \times 10^3, 2 \times 10^4)$
2	K	sb_kratio	Normal to shear stiffness ratio	(1, 10)
3	m	sb_rmul	Radius multiplier	(0.2, 2)
4	fr	sb_ref_str	Reference strength of soft bond (MPa)	(40, 100)
5	r_{min}	rmin	Minimum particle radius (mm)	(0.05, 0.5)
6	α_a	alpha_a	Ratio of maximum to minimum particle radius	(1, 1.5)
7	β	beta	Ratio of tensile to cohesion strength	(0.1, 1)

(2) Standard DE models for running the numerical uniaxial tests were assigned with the above 300 groups of adjustable parameters to obtain 300 models. The results of the target properties can then be extracted after running these 300 models.

In the standard DE model, the expansive particle packing method was used to generate the adhesives. Small particles were randomly generated in the defined area and gradually expanded to contact neighboring particles. Once introducing the soft bond model after completing particle packing, the model can be ready to be loaded till failure. The load speed of grip was determined to be 0.1 m/s after a sensitivity study of load speed. Two layers of particles at the left and right edges were selected as grip to impose tensile load. An example of standard DE model and the corresponding screenshot at failure is given in Fig. 1, in which the tearing can be seen near the specimen center.

The collection of engineering stress-strain relationship from the virtual experiments on brittle adhesives was shown in Fig. 2.The maximum and minimum values of the secant modulus (E_s) were also given. It is found that the collected data can cover a wide range of stiffness, tensile strength and failure strain seen in brittle adhesives. The nonlinearity of the stress-strain curves can also be observed.

2.3. Configuration of GEP model

In order to find practical formulas to roughly approximate the results of the target properties using the selected adjustable microscopic parameters, a symbolic regression (SR) model was adopted. SR model seeks to capture a function $\boldsymbol{f(X)} = \boldsymbol{Y'}$, which can minimize the deviation between predicted property $\boldsymbol{Y'}$ and target property $\boldsymbol{Y}$. $\boldsymbol{X}$ is the dataset of adjustable DE parameters. The function is determined via a continuous optimization to the best fit based on the symbols from the predefined space of mathematical expressions. In this work, a variant of genetic programming (GP) algorithm, GEP, was used to find the best fit through employing the crossover and mutation of function structures [40].

GP algorithm has been widely used in finding the optimized regression model in a wide range of topics, e.g., to estimate the compressive strength of rock [41,42] or predict the failure strength of adhesive joints [43,44]. Its variant, GEP algorithm, encodes the individuals as linear strings of fixed length which are subsequently expressed as nonlinear entities of different sizes and structures [45]. The GEP structure encompasses two components, a head having function symbols and terminal symbols (e.g., adjustable parameters, coefficients), and a tail having terminal symbols. In a standard GEP procedure, it begins with the stochastic generation of the chromosomes of the initial population. The chromosomes are then translated and expressed, followed by the evaluation of the fitness of each individual. The procedure will be looped until ending with a defined number of generations or finding a reliable solution.

The datasets of the adhesive had 300 groups of adjustable microscopic parameters and extracted target properties from the DE models. 2/3 of the datasets were randomly selected for training and the remaining were used for validation. The parameter configuration of the

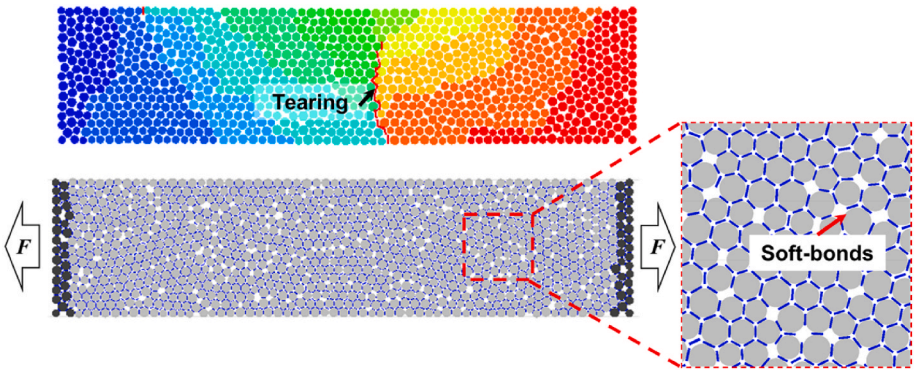

Fig. 1. Standard DE model of uniaxial tensile test on adhesives.

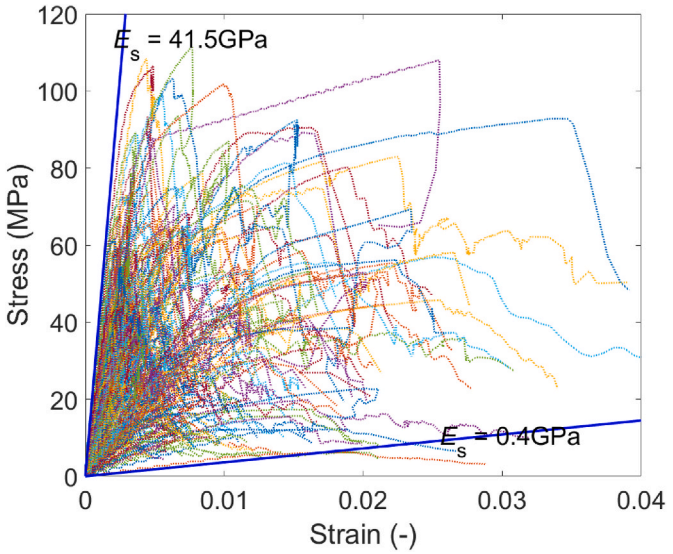

Fig. 2. Stress-strain results of DEM virtual experiment.

GEP algorithm in this work as well as the enabled symbols are listed in Table 3.

The comparison between the target properties and predicted results of the SR model by GEP algorithm is shown in Fig. 3. Linear fitting is used to fit the data. It can be seen that most SR models can obtain a value of R^2 around 0.9 or above, indicating a satisfactory prediction. However, although great efforts were made to achieve the optimized fitness of the SR model, several data points showing high dispersion from the predicted results can still be found. The odd data points are due to the specific set up of measure point on DE model, which is found to be near to the tearing position of the adhesive unexpectedly in few cases. However, those odd cases were still considered in GEP model to include the generality of datasets. Therefore, the coefficient of determination R^2 might not be ideal in certain cases, in particular, the case for predicting the peak strain of brittle adhesive (see Fig. 3(a1, a2)). Fig. 4 shows the residual plots of the peak strain results in training and validation groups. It is seen that most of results are closely neighboring to zero value, whereas the variance has a trend to be non-constant when the strain grows.

Table 3
Configuration of GEP algorithm.

Parameters	Value (Range)
Number of chromosomes	30
Head size, number of genes	8, 3
Training/Validation records	200/100 (total 300)
Enabled symbols	$+, -, \times, /, e^x, 10^x, \ln x, \lg x, \lvert x\rvert, 1/x, x^i, \sqrt[i]{x}(i = 2, 3, 4\ldots)$, $\tanh, \tan^{-1}$

2.4. Symbolic regression models for bulk property

The formulas from the determined SR models to predict the target properties of brittle adhesives are given in Eqs. (3)–(5), respectively. The units of the adjustable parameters are consistent with those in Table 2.

$$\text{Peak strain, } (-)\quad \varepsilon_p = \tanh(\ln f_r - \ln E_m/1.1 + \tanh(r_{min})) - E_m + 1\Big/\left(10^{\beta} - (K - 14.4) + \sqrt{E_m}\right) + E_m + \left(\tanh\left(\ln\sqrt{2.18 f_r} \times \sqrt{\tanh(\alpha_a)}\right)\right)^{1/5} \tag{3}$$

$$\text{Tensile strength, (MPa)}\quad f_t = (\ln(8.21 + 106.3/f_r) - m)^4 + \tan^{-1}(m)((K - f_r) \times (9.27 + m))^{2/3} + m^{(f_r/\alpha_a)^{1/3}} - 25.13 \tag{4}$$

$$\text{Secant modulus at strain of 0.001, (MPa)}\quad E_s = 45 m f_r/K - 103.7\alpha_a K + 695/\ln\left(10^{r_{min}} r_{min} + \alpha_a{}^5\right) + 368.5 m\beta + m E_m - 100 r_{min} K^m \tag{5}$$

As the ratio of tensile to cohesion strength, β, was a parameter related to shear strength, it was not adopted to perform the following sensitivity study. The other six adjustable parameters were selected in this study to examine the influences of each parameter on the target properties. The parameters were constant (see Table 4 for brittle adhesive) if they were not the examined one, whilst the examined parameters were assigned with a range identical to those in Table 2. The target properties were calculated based on the developed SR models. The calculated ranges of the target properties, peak strain, tensile strength and secant modulus at strain of 0.001 in brittle adhesives were shown in Fig. 5 (a1-a3), Fig. 5 (b1-b3), Fig. 5 (c1-c3), respectively. The projections of the target properties on the planes with constant maximum assigned values of parameters were also given to better clarify the correlation trend (see contours without mesh grid).

From Fig. 5 (a1-a3), it is seen that in the defined interval, effective modulus (e_mod, E_m) and reference strength (sb_ref_str, f_r) contribute more to the peak strain. The former can generate a maximum strain increment around 0.015 within its assigned interval. The latter can achieve a strain range of (0.0084, 0.0166), i.e. a strain increment of 0.0082. The other parameters present less influence on the strain increment, which varies from 0.00136 for minimum particle radius (r_{min}) to 0.003 for normal to shear stiffness ratio (sb_kratio, K). In Fig. 5 (a2), radius multiplier (rmul, m) is not included in the SR model for strain, thus, it is without change when f_r varies.

From Fig. 5 (b1-b3), the reference strength f_r and radius multiplier m

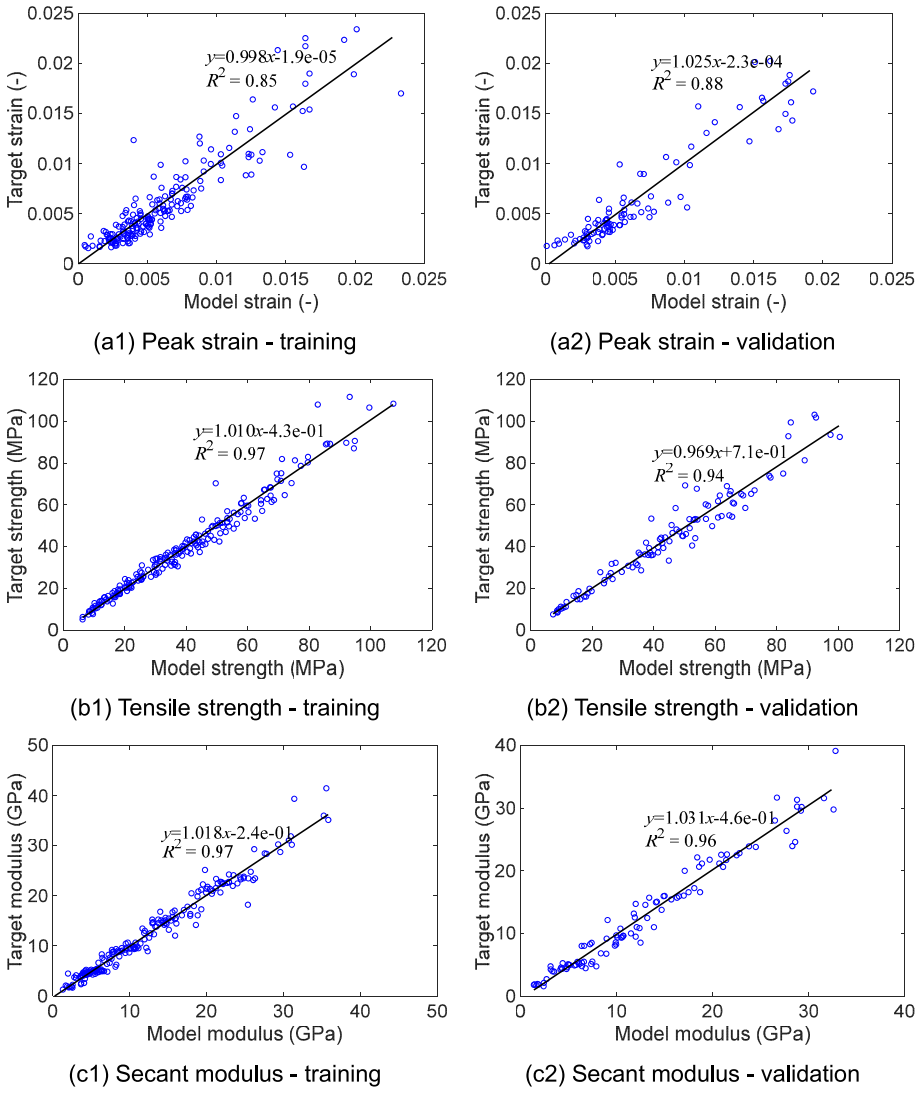

Fig. 3. Comparison of target and predicted results for brittle adhesives.

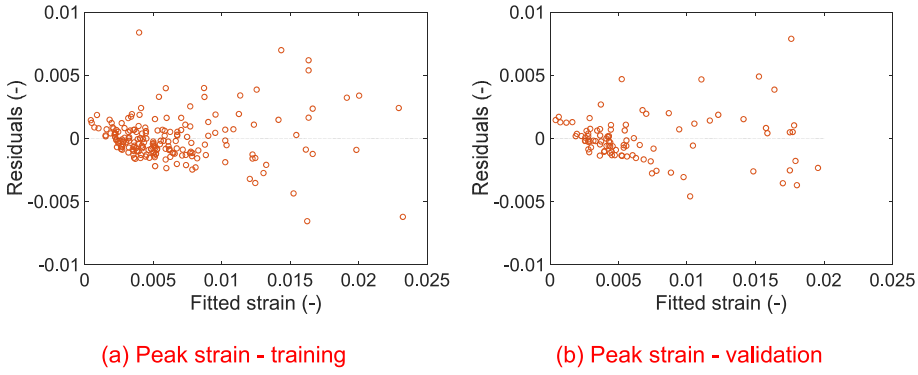

Fig. 4. Residual plots of training and validation results of peak strain.

are predominant in determining the tensile strength, showing a maximum strength increment of around 66 MPa and 100 MPa, respectively. The strength increment by adjusting K and E_m is within 10 MPa, whilst that by α_a and r_{min} decreases to only 2 MPa (Fig. 5 (b3)). From Fig. 5 (c1-c3), it is seen that E_m and m contribute the most to the secant modulus, of which the maximum modulus increments within the defined intervals are 34 GPa and 9 GPa, respectively. The parameters, K and f_r, can be used to perform the fine adjustment of secant modulus, as their modulus increments have a smaller range of 1.5 GPa–5.6 GPa. The influences due to the parameters, α_a and r_{min}, are negligible within most of their interval. However, the modulus increment will see a significant rise to nearly 12.5 GPa when both α_a and r_{min} decrease to the defined minimum values (Fig. 5 (c3)). This might be due to that the denser packing via decreasing α_a and r_{min} is more likely to generate stiffer

Table 4
Assigned values of adjustable parameters for brittle adhesive.

Symbol	Keyword	Values	Symbol	Keyword	Values
E_m	sb_emod	3.65 GPa	r_{min}	rmin	0.1 mm
K	sb_kratio	3.6	α_a	alpha_a	1.33
m	sb_rmul	1.9	β	beta	0.25
fr	sb_ref_str	46.3 MPa			

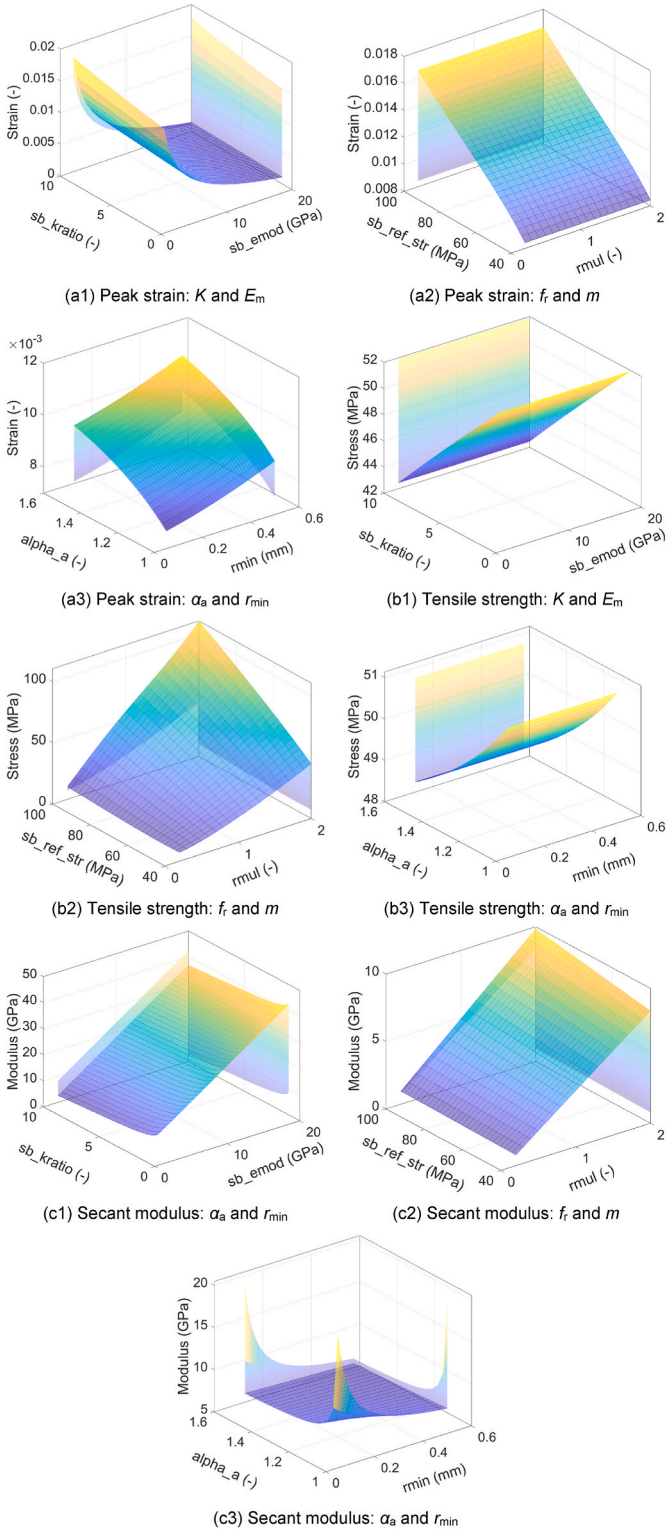

Fig. 5. Predicted results using regression formulas of brittle adhesives.

material.

Overall, once the target properties of adhesives from experimental results have been determined. For each target property, the parameters contribute the most to the corresponding property can be adjusted and then fixed to achieve a close value to the target one. The other parameters having less influences on this property can then be adjusted to refine the target value until the parameter set can determine similar properties to the target values.

2.5. Validation of estimated parameters

In order to provide experimental data for the determination of the microscopic parameters, uniaxial tensile (UT) tests were subsequently conducted to record the stress-strain relationships of adhesives. Brittle epoxy (Loctite EA 9497) was used to make the dumb-bell shaped UT specimens following the ISO 527-2 [46] standard. Digital image correlation (DIC) technique was used to measure the strain field of the adhesive specimens. The universal tensile machine Instron 3345 equipped with a 5 kN load cell was used to perform the tensile tests on the specimens. Three specimens were tested to guarantee the repeatability.

Using the developed SR models of adhesives and the developed calibration procedure of adjusting microscopic parameters, the microscopic parameters of the adhesives were determined to generate the macroscopic behaviour that agrees well with the experimental target. The determined parameters are given in Table 4. The reproduced numerical and experimental stress-strain curves are shown in Fig. 6. It can be seen that the determined microscopic parameters are reliable.

3. Interlaminar-like property of thin adhesives in joints

Comparing with the thick adhesive, thin adhesive is more commonly used in joint design. In this case, the interlaminar-like properties such as the fracture energy are more concerned to be reproduced in DE model. This is due to that the actual performance of adhesive is influenced by the adhesive thickness, constraints from adherends etc., the bulk property cannot be directly used to simulate the actual property of a thin adhesive layer between adherends. In this section, the microscopic parameters were adjusted to suit the interlaminar-like behavior of thin adhesive from the lab tests. The equivalent fracture energy in normal and tangential directions, which were generated by the cohesive fracture of thin adhesive, were treated as the target properties.

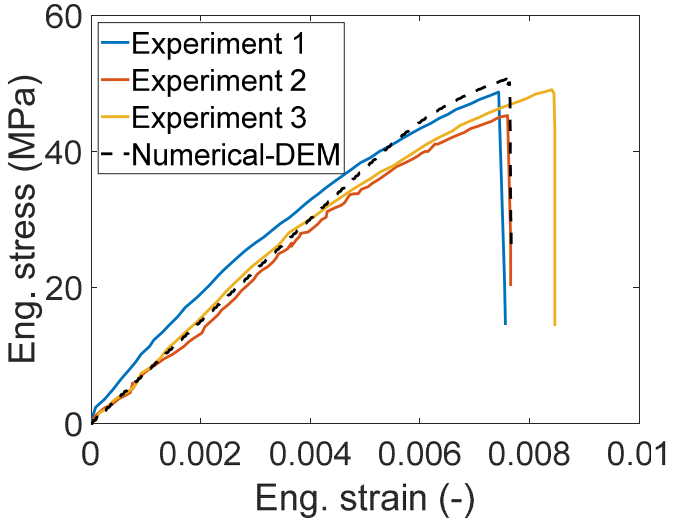

Fig. 6. Comparison between the numerical and experimental results of adhesives.

3.1. Virtual experiment on determining interlaminar-like property

Before performing the virtual experiment, the actual experiment on the interlaminar-like behaviour of laminates using brittle epoxy (Loctite EA 9497) was conducted to provide reference data. It is well known that the adherend stiffness and the adhesive thickness will affect the fracture strength and fracture energy. Thus, a fixed configuration was determined with aluminium (AL) adherends and 0.56 mm thick adhesive. DCB and ENF tests were adopted to obtain the Mode I and Mode II interfacial properties, respectively. The extracted interfacial properties from the cohesive failure of adhesive layer were given in Table 5, more information can be found in Ref. [9].

The failure modes of adhesive joints are generally classified into three categories, adhesive failure, cohesive failure and mix mode failure. In this work, the thin adhesive is assumed to present consistent cohesive failure. In fact, in most joints using strong adherends, adhesive failure might be less likely to occur if high quality treatment and the cleaning of adherend surfaces can be guaranteed. This can also be supported by the above DCB and ENF tests, which typically had cohesive failure mode. For calibrating the interlaminar-like property in normal direction, a simplified virtual experiment having a joint under uniaxial tension was performed as shown in Fig. 7 (a). The configuration of bonding to half of the interface was designed to reduce the effect by the model edge on the stress/strain field near the adhesive under tension. The bonds between epoxy balls and adherend balls (AL) were set to be unbreakable to trigger the cohesive failure. Hexagonal packing with soft bond model was employed for the adherend (AL) in this model, in which the parameters were determined based on the theoretical solutions in Ref. [47]. Tensile action was imposed on the right edge of adherend until the epoxy tearing propagated through the entire adhesive layer. The fracture energy can be calculated by the integral of tensile stress and relative displacement between two reference balls at the interface. Similar strategy was employed for the model to calibrate the tangential interlaminar-like property in Fig. 7 (b). A simplified double shear-type connection was used to evaluate the fracture energy under shear action.

3.2. Sensitivity study and GEP modelling

As mentioned above, the fracture strength and energy of a thin adhesive layer are not same as those in a bulk adhesive material due to the effects by the constraints and adhesive thickness. For instance, it can be seen in Table 5 that the normal cohesive strength of the epoxy adhesive is much lower than the tensile strength from uniaxial tensile tests. Furthermore, current study shows that the fracture energy is the predominant factor controlling the failure load of a thin adhesive joint [20,48]. It indicates that even parameters related to the strength of adhesive should be adjusted to obtain the reduction of cohesive strength. It is noting that a sensitivity study on the particle size of adherend and adhesive should be conducted to determine an appropriate particle size used in the later simulations.

(1) Sensitivity study on particle size

Firstly, a sensitivity study of the ratio ω of adherend particle radius to that of adhesive was conducted. It is expected that a larger ratio ω will result in more local fractures of adhesive bonds and neglect the contribution of adhesive balls between two adherend particles, which might generate lower fracture strength and fracture energy. Therefore, a suitable ratio ω and associated particle radius were then determined for the following virtual experiment on interlaminar-like property. The tested parameters were given in Table 6. Epoxy adhesive was selected in this study, of which most material parameters were identical to those in Table 4, except for that the reference strength was reduced to the mean normal fracture strength of Loctite EA 9497 (25.35 MPa) from Table 5. The normal stress and fracture energy from cases with radius ratio from 2 to 16 were obtained and shown in Fig. 8 (a), (b), respectively.

It can be seen from Fig. 8 that, the results from cases with adhesive particle radius of 0.025 mm and 0.05 mm have high consistency before the initiation of adhesive tearing. The difference of normal stress subsequently sees a rise (Fig. 8 (a)), however, the fracture energy will finally grow to a close value in the case with identical radius ratio. Higher consistency can be achieved as the radius ratio decreases, i.e. the particles of adherends and adhesives have more bonding areas. Although the normal stress is higher in the case with a ratio of 2, it is found that the difference in the fracture energy between the ratios of 2 and 4 is negligible, which indicates that a radius ratio of 4 is adequate to simulate the problem that is more related to the fracture energy. Therefore, the following study will employ a radius ratio of 4 and a minimum ball radius of 0.05 mm for adhesive to reduce the computation cost.

(2) GEP modelling for interlaminar-like properties

Artificial adjustment was subsequently performed to determine a suitable parameter set for simulating the fracture behavior of thin adhesive layer. It was expected that the fine adjustment can guarantee the interlaminar-like property without the significant variation of determined parameters for bulk property. However, it is found that great difficulties rise in reaching this aim, thus, the following strategy was adopted: the parameters related to the elasticity of adhesive were not adjusted, whilst the adhesive strength was allowed to vary. The strategy has the priority to guarantee the fracture energy, which dominates the performance of thin adhesive joints.

The discussion in Section 2.3 concludes that the parameters E_m (effective modulus) and m (radius multiplier) have significant influence on the secant modulus, i.e. they need to be fixed. The parameters K (normal to shear stiffness ratio) and fr (reference strength) have much less effect and were taken as adjustable parameters for the interlaminar-like property. In addition, β (the ratio of tensile to cohesion strength) has negligible effect on the tensile behavior of bulk adhesive as it is designed to coordinate the shear behavior. It was also adopted as it contributes to the Mode II fracture behavior of thin adhesive joint.

A similar procedure to the characterization process of bulk adhesive was used to obtain the SR models of target properties, Mode I and Mode II fracture energies, based on three adjustable parameters. Through trial virtual experiment, the parameters K, β were assigned with a range of (1, 10) and (0.2, 3.0), respectively. The reference strength fr had a range of (10, 30) for brittle adhesive. The other parameters were identical to those from Table 4. LHS method was then adopted to produce 100 groups of parameters to run the virtual tests based on the models from Fig. 7.

The obtained Mode I fracture energy covers a range from 0.04 N/mm to 1.42 N/mm and Mode II fracture energy varies from 0.04 N/mm to 3.04 N/mm. The range of fracture energy can cover the tested data from the commonly used adhesives and is able to be used in the subsequent GE modelling. The configuration of GE model for regressing the relationship of fracture energy and selected three parameters was same as that in Table 3, except for that the training and validation records were 100.

Fig. 9 gives the training and validation results of the regressed SR model for brittle adhesive. It can be found that the regressed model can well predict the Mode I and Mode II fracture energies from the virtual experiment, as the values of R^2 are higher than 0.94 in both training and validation results. It is worth noting that the training results in Fig. 9 (b1) are more scattering, which is related to the threshold of calculating the fracture energy. In DE models, to obtain Mode II fracture energy, the

Table 5
Interfacial properties extracted from actual experiment.

Property	Symbol	Loctite EA 9497 (AL-AL)
Normal Fracture energy	G_{IC} (N/mm)	0.26 ± 0.06
Tangential Fracture energy	G_{IIC} (N/mm)	0.90 ± 0.39
Normal fracture strength	σ_n (MPa)	25.35 ± 10.26
Tangential fracture strength	σ_t (MPa)	16 ± 5

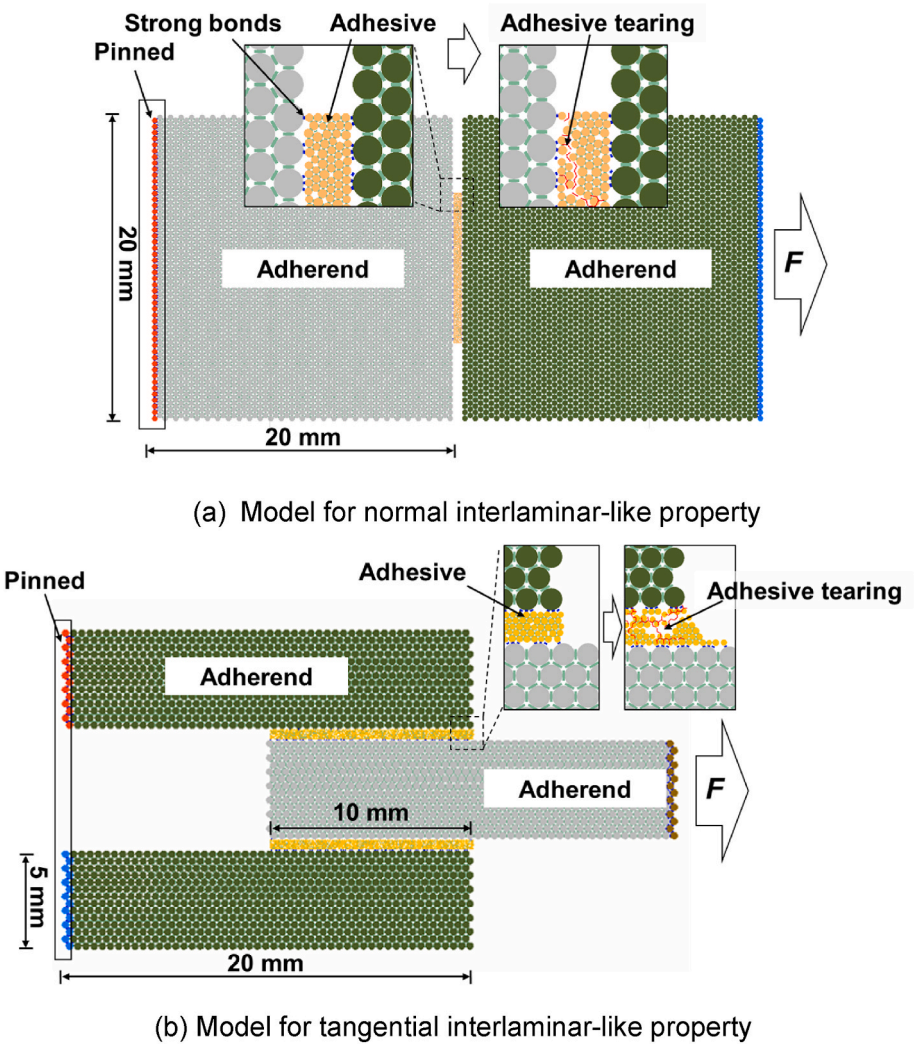

Fig. 7. DE models for the calibration of interlaminar-like property.

Table 6
The parameters for the sensitivity study of particle radius ratio.

Parameters	Particle radius ratio ω	Minimum particle radius of adhesive, r_{min}, mm
Values	2, 4, 8, 16	0.025, 0.05

threshold of determining the Mode II fracture energy was 10% of the peak stress. However, it is found that before declining to zero the shear stress might reach a plateau of low stress value over threshold with several parameter combinations, which will accumulate the Mode II fracture energy. Thus, the artificially determined threshold will generate different fracture energies. Overall, in most combinations of parameters, the threshold of 10% peak stress was adequate to obtain reliable fracture energies.

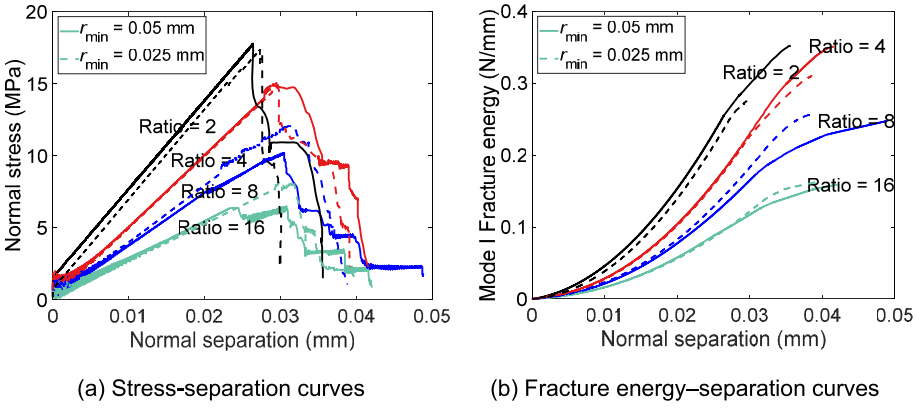

Fig. 8. Results of the sensitivity study.

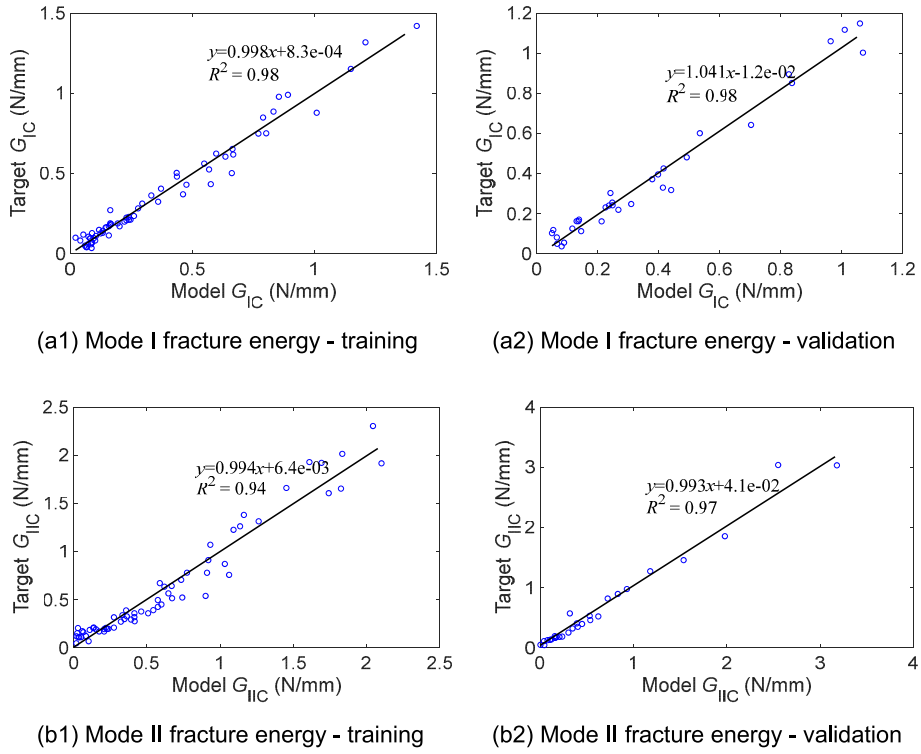

Fig. 9. Target and predicted results for interlaminar-like property of brittle adhesives.

3.3. Symbolic regression models for interlaminar-like property

The following equations (6) and (7) were given to predict the target normal and tangential fracture energies of brittle adhesives.

$$\text{GIC}\ \ (\text{N/mm})\quad G_{\text{IC}} = \left(\left(|f_{\text{r}}| - 15.5\beta\right)\left(f_{\text{r}} - \beta^2\right) + \left(5.47 - \beta\right)\left(12.3 + f_{\text{r}}\right)\left(f_{\text{r}} + 1/\beta\right)/10 + \left(122.8 + \beta^3\right) - \left(2.48K/\beta^2\right)\right)/10^3 \tag{6}$$

$$\text{GIIC}\ \ (\text{N/mm})\quad G_{\text{IIC}} = 1.5\left(\left(f_{\text{r}}^2 - 259/\beta\right) + 12.25\beta\left(K - f_{\text{r}}\right) + \ln\left(\ln\left(f_{\text{r}}\right)\right)\left(e^{(7.4-\beta)} - f_{\text{r}} + K\right) + \left(f_{\text{r}} - \beta\right)\left(f_{\text{r}} - 1.93K\right)/\beta\right)/10^3 \tag{7}$$

The calculated ranges of Mode I and Mode II fracture energies (take β = 0.25, 1.5 as example) by the above SR models are given in Fig. 10 (a) and (b), respectively. It can be seen that by varying β, the interval of simulated fracture energy can be adjusted within the given range of fr

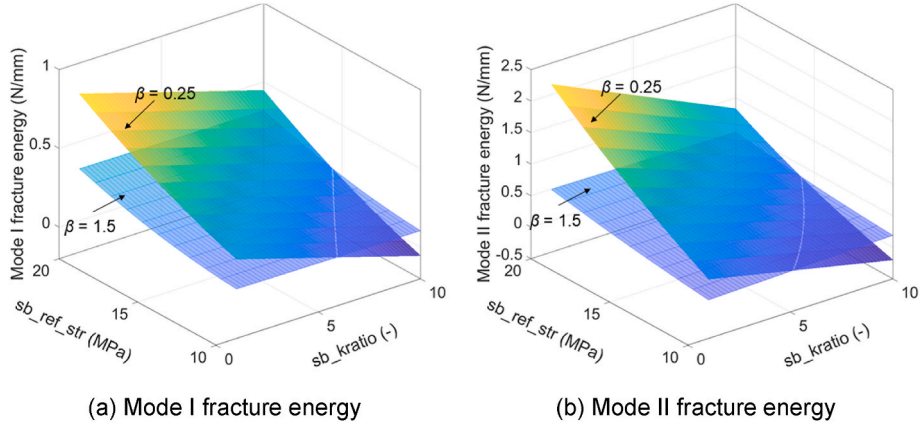

Fig. 10. Predicted fracture energy using regression formulas of brittle adhesives.

and K. Once the experimental fracture energy was obtained, the corresponding parameters can be determined by fixing one parameter and locating the combination of other two parameters which can achieve the closest fracture energy to the experimental value. However, as mentioned above, the threshold of stopping simulation will affect the calculated fracture energy. It is found that a very low threshold is recommended to obtain more accurate fracture energy in an ideal model. However, it might be very difficult to reach the threshold and the computation cost to collect the database for GE modelling is expected to be very high. In this work, the threshold of 10% peak stress might still underestimate the simulated fracture energy. The determination of parameters is suggested to consider this issue, a slight lower value of fracture energy can be estimated and used to locate the parameter combination.

3.4. Parameters determination and validation

DCB and ENF tests were adopted to validate the determined parameter sets for a thin adhesive made of epoxy (Loctite EA 9497) adhesive. Fig. 11 shows the DE models of DCB and ENF tests. The adhesive thickness was 0.56 mm. The experimental information can be found in Ref. [49]. The load speed was determined as 0.05 m/s for each test after a sensitivity study on load speed. The assigned values of parameters for epoxy adhesive are determined as: 4.70 for K (sb_kratio), 14.0 MPa for fr (sb_ref_str) and 1.0 for β (beta). The other parameters of soft bond model are identical to those for bulk property.

The comparison of experimental and numerical results in DCB and ENF tests is shown in Fig. 12. In Fig. 12 (a), it is found that once the cohesive fractures of the epoxy adhesive propagate, the oscillation of reaction force can be seen due to the dynamic effect at fracturing process. The oscillation can be reduced by decreasing the load speed, which was artificially increased to reduce computation cost in this work. From Fig. 12 (b), it is seen that the DE model can achieve satisfactory results in modelling the ENF test on the epoxy adhesive, although the linear stiffness of DE model is lower than that from the experimental data. As the displacement at peak load in ENF test on epoxy is very small (nearly 1.0 mm), it is difficult to obtain an accurate value by using current testing apparatus, e.g., the displacement at peak load from other sensors is nearly 1.5 mm. Therefore, the simulated load-displacement results are rational considering this issue. In summary, the overall load-displacement curves of DCB and ENF tests from the DEM simulation are consistent with those from the experimental data.

A micromechanical model which used the SLJ as the example was developed to examine its reliability in predicting the failure process. Differing from the DCB and ENF tests where the adhesives are under single mode loading action, the adhesive in SLJ is subjected to combined tensile and shear actions. Thus, the modelling reliability of mixed mode behaviour of adhesive is worthy of investigation. The geometrical details of the SLJ model were shown in Fig. 13(a) with the cohesive fractures of the adhesive highlighted. AL adherend and epoxy (Loctite EA 9497) adhesive were used to make the specimens which were experimentally tested to provide the data for validation. Three SLJ specimens were tested.

The comparison of the experimental and numerical results was given in Fig. 13(b). It is seen that the DE model can achieve a satisfactory consistency of numerical prediction to the testing data. All the characteristics of load-displacement relationships such as the failure load, stiffness before failure agree well with the experimental results, indicating the applicability of the developed micromechanical model in simulating the load scenarios with mixed mode behaviours of adhesive joints.

4. Conclusions

This work developed a characterization procedure for the microscale parameters of particle-based model in modelling brittle adhesives in joint design. A practical approach encompassing the virtual experiment using discrete element modelling and the genetic expression programming technique was adopted to obtain the symbolic regression models, which can facilitate the estimation of the bulk property of thick adhesive and the interlaminar-like property of thin adhesive. The applicability of the estimated parameters and the micromechanical model was examined by comparing with those from various lab tests of selected brittle adhesives. The key findings are listed below:

(1) Practical regression models for estimating the bulk properties of thick adhesive, including tensile strength, peak strain, secant modulus, and the interlaminar-like properties of thin adhesive, i.e. Mode I and Mode II fracture energy, were developed to roughly estimate the microscale parameters. The models can cover a wide range of brittle adhesives.
(2) The developed model using estimated microscale parameters can well predict the micromechanical behaviour of brittle adhesives under different loading scenarios including the mixed mode behaviours.

The developed estimation approach and the micromechanical model are expected to be capable of adaptively capturing the variation of

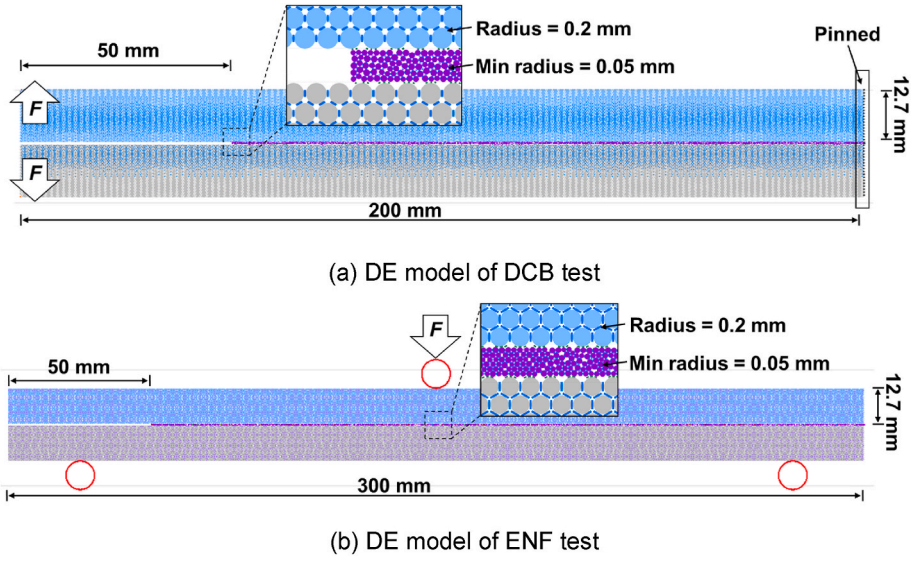

Fig. 11. DE models of DCB and ENF tests.

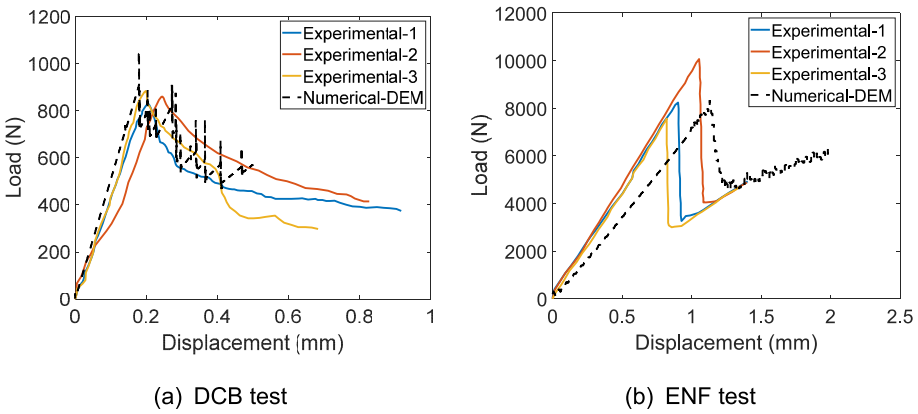

Fig. 12. Comparison of experimental and numerical results of DCB and ENF tests.

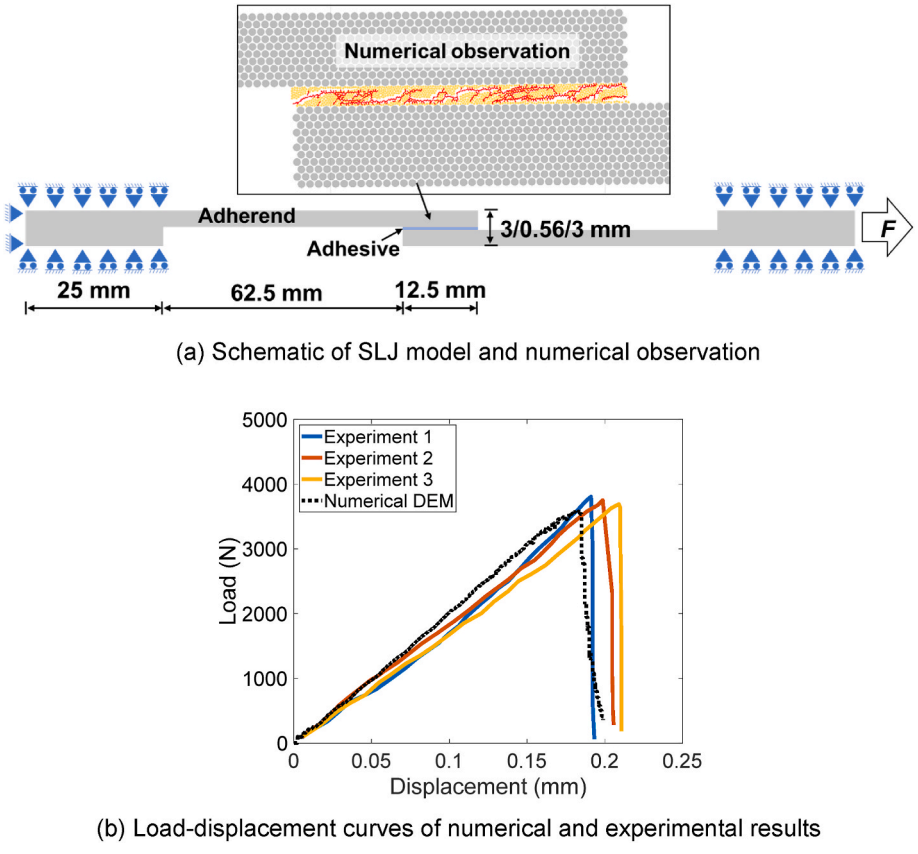

Fig. 13. SLJ model and the validation results.

fracture energy of adhesive joints when using different design variables such as adhesive thickness, adherend materials etc. This can save more efforts to perform associated experiment to extract the cohesive parameters.

CRediT author statement

Xing-er Wang: Writing – Original Draft, Investigation. **Armin Yousefi Kanani:** Investigation, Validation, Data curation. **Zewen Gu**: Software, Formal analysis. **Jian Yang:** Writing - Review & Editing. **Jianqiao Ye** : Writing - Review & Editing, Supervision. **Xiaonan Hou**: Investigation, Writing – Review & Editing, Supervision, Project administration, Funding acquisition.

Declaration of competing interest

The authors declare that they have no known competing financial interests or personal relationships that could have appeared to influence the work reported in this paper.

Acknowledgement

This study was funded by the Engineering and Physical Sciences Research Council, UK [Grant No. EP/T020695/1]. The authors would like to acknowledge Henkel Ltd. for the technical support and providing adhesive specimens.

References

[1] Lyathakula KR, Yuan F-G. A probabilistic fatigue life prediction for adhesively bonded joints via ANNs-based hybrid model. Int J Fatig 2021;151:106352. https://doi.org/10.1016/j.ijfatigue.2021.106352.

[2] Jojibabu P, Zhang YX, Rider AN, Wang J. Mechanical performance of adhesive joints using high-performance nanocomposite adhesive material with carbon nanotube and triblock copolymer hybrids. Compos B Eng 2020;186:107813. https://doi.org/10.1016/j.compositesb.2020.107813.

[3] Huang X-H, Wang X-e, Yang J, Pan Z, Wang F, Azim I. Nonlinear analytical study of structural laminated glass under hard body impact in the pre-crack stage. Thin-Walled Struct 2021;167:108137. https://doi.org/10.1016/j.tws.2021.108137.

[4] Delzendehrooy F, Ayatollahi MR, Akhavan-Safar A, da Silva LFM. Strength improvement of adhesively bonded single lap joints with date palm fibers: effect of type, size, treatment method and density of fibers. Compos B Eng 2020;188:107874. https://doi.org/10.1016/j.compositesb.2020.107874.

[5] Wagih A, Tao R, Lubineau G. Bio-inspired adhesive joint with improved interlaminar fracture toughness. Compos Appl Sci Manuf 2021;149:106530. https://doi.org/10.1016/j.compositesa.2021.106530.

[6] Boutar Y, Naïmi S, Mezlini S, Carbas RJC, da Silva LFM, Ben Sik Ali M. Fatigue resistance of an aluminium one-component polyurethane adhesive joint for the automotive industry: effect of surface roughness and adhesive thickness. Int J Adhesion Adhes 2018;83:143–52. https://doi.org/10.1016/j.ijadhadh.2018.02.012.

[7] Tan W, Na J, Wang G, Xu Q, Shen H, Mu W. The effects of service temperature on the fatigue behavior of a polyurethane adhesive joint. Int J Adhesion Adhes 2021;107:102819. https://doi.org/10.1016/j.ijadhadh.2021.102819.

[8] Marchione F, Munafò P. Experimental investigation on timber-glass double-lap adhesive joints reinforced with nylon fabric. Construct Build Mater 2021;275:122152. https://doi.org/10.1016/j.conbuildmat.2020.122152.

[9] Kanani AY, Liu Y, Hughes DJ, Ye J, Hou X. Fracture mechanisms of hybrid adhesive bonded joints: effects of the stiffness of constituents. Int J Adhesion Adhes 2020;102:102649. https://doi.org/10.1016/j.ijadhadh.2020.102649.

[10] Yang J, Wang Y, Wang X-e, Hou X, Zhao C, Ye J. Local bridging effect of fractured laminated glass with EVA based hybrid interlayers under weathering actions. Construct Build Mater 2022;314:125595. https://doi.org/10.1016/j.conbuildmat.2021.125595.

[11] Wang X-E, Meng Y, Yang J, Huang X, Wang F, Xu H. Optimal kernel extreme learning machine model for predicting the fracture state and impact response of laminated glass panels. Thin-Walled Struct 2021;162:107541. https://doi.org/10.1016/j.tws.2021.107541.

[12] Shah OR, Tarfaoui M. Effect of adhesive thickness on the Mode I and II strain energy release rates. Comparative study between different approaches for the calculation of Mode I & II SERR's. Compos B Eng 2016;96:354–63. https://doi.org/10.1016/j.compositesb.2016.04.042.

[13] Sancaktar E, Karmarkar U. Mechanical behavior of interlocking multi-stepped double scarf adhesive joints including void and disbond effects. Int J Adhesion Adhes 2014;53:44–56. https://doi.org/10.1016/j.ijadhadh.2014.01.012.

[14] Sengab A, Talreja R. A numerical study of failure of an adhesive joint influenced by a void in the adhesive. Compos Struct 2016;156:165–70. https://doi.org/10.1016/j.compstruct.2015.12.052.

[15] Kanani AY, Hou X, Laidlaw R, Ye J. The effect of joint configuration on the strength and stress distributions of dissimilar adhesively bonded joints. Eng Struct 2021;226:111322. https://doi.org/10.1016/j.engstruct.2020.111322.

[16] Dionísio JMM, Ramalho LDC, Sánchez-Arce IJ, Campilho RDSG, Belinha J. Fracture mechanics approach to stress singularities in composite adhesive joints. Compos Struct 2021;276:114507. https://doi.org/10.1016/j.compstruct.2021.114507.

[17] Wang X-e, Huang X-H, Yang J, Hou X, Zhu Y, Xie D. Experimental and analytical study on the pre-crack impact response of thick multi-layered laminated glass under hard body impact. Int J Mech Sci 2021;206:106613. https://doi.org/10.1016/j.ijmecsci.2021.106613.

[18] Wang X-e, Yang J, Wang F, Liu Q-f, Xu H. Simulating the impact damage of laminated glass considering mixed mode delamination using FEM/DEM. Compos Struct 2018;202:1239–52. https://doi.org/10.1016/j.compstruct.2018.05.127.

[19] Chen S, Mitsume N, Gao W, Yamada T, Zang M, Yoshimura S. A nodal-based extrinsic cohesive/contact model for interfacial debonding analyses in composite structures. Comput Struct 2019;215:80–97. https://doi.org/10.1016/j.compstruc.2019.02.001.

[20] Kim M-H, Ri U-I, Hong H-S, Kim Y-C. Comparative study of failure models for prediction of mixed-mode failure characteristics in composite adhesively bonded joint with brittle/Quai-brittle adhesive using finite element analysis. Int J Adhesion Adhes 2021;109:102911. https://doi.org/10.1016/j.ijadhadh.2021.102911.

[21] Shi J-W, Cao W-H, Wu Z-S. Effect of adhesive properties on the bond behaviour of externally bonded FRP-to-concrete joints. Compos B Eng 2019;177:107365. https://doi.org/10.1016/j.compositesb.2019.107365.

[22] Al-Ramahi NJ, Joffe R, Varna J. Numerical analysis of stresses in double-lap adhesive joint under thermo-mechanical load. Eng Struct 2021;233:111863. https://doi.org/10.1016/j.engstruct.2021.111863.

[23] Liu PF, Peng XQ, Guo ZY, Leng JX, Jiao L. Viscoelastic bilinear cohesive model and parameter identification for failure analysis of adhesive composite joints. Compos Struct 2019;224:111016. https://doi.org/10.1016/j.compstruct.2019.111016.

[24] Alves DL, Campilho RDSG, Moreira RDF, Silva FJG, da Silva LFM. Experimental and numerical analysis of hybrid adhesively-bonded scarf joints. Int J Adhesion Adhes 2018;83:87–95. https://doi.org/10.1016/j.ijadhadh.2018.05.011.

[25] Kaiser I, Tan KT. Damage and strength analysis of Carbon Fiber Reinforced Polymer and Titanium tubular-lap joint using hybrid adhesive design. Int J Adhesion Adhes 2020;103:102710. https://doi.org/10.1016/j.ijadhadh.2020.102710.

[26] Çavdar S, Teutenberg D, Meschut G, Wulf A, Hesebeck O, Brede M, et al. Stress-based fatigue life prediction of adhesively bonded hybrid hyperelastic joints under multiaxial stress conditions. Int J Adhesion Adhes 2020;97:102483. https://doi.org/10.1016/j.ijadhadh.2019.102483.

[27] Sun F, Pruncu CI, Penchev P, Jiang J, Dimov S, Blackman BRK. Influence of surface micropatterns on the mode I fracture toughness of adhesively bonded joints. Int J Adhesion Adhes 2020;103:102718. https://doi.org/10.1016/j.ijadhadh.2020.102718.

[28] Pizzorni M, Lertora E, Parmiggiani A. Adhesive bonding of 3D-printed short- and continuous-carbon-fiber composites: an experimental analysis of design methods to improve joint strength. Compos B Eng 2022;230:109539. https://doi.org/10.1016/j.compositesb.2021.109539.

[29] Akman E, Bora MÖ, Çoban O, Oztoprak BG. Laser-induced groove optimization for Al/CFRP adhesive joint strength. Int J Adhesion Adhes 2021;107:102830. https://doi.org/10.1016/j.ijadhadh.2021.102830.

[30] Zhang D, Huang Y. Influence of surface roughness and bondline thickness on the bonding performance of epoxy adhesive joints on mild steel substrates. Prog Org Coating 2021;153:106135. https://doi.org/10.1016/j.porgcoat.2021.106135.

[31] Gong L, Nie L, Xu Y, Wang H, Zhang T, Du C, et al. Discrete element modelling of the mechanical behaviour of a sand-rubber mixture containing large rubber particles. Construct Build Mater 2019;205:574–85. https://doi.org/10.1016/j.conbuildmat.2019.01.214.

[32] Cheng Z, Wang J, Li W. The micro-mechanical behaviour of sand–rubber mixtures under shear: an experimental study based on X-ray micro-tomography. Soils Found 2020;60(5):1251–68. https://doi.org/10.1016/j.sandf.2020.08.001.

[33] Yu M, Yang B, Chi Y, Xie J, Ye J. Experimental study and DEM modelling of bolted composite lap joints subjected to tension. Compos B Eng 2020;190:107951. https://doi.org/10.1016/j.compositesb.2020.107951.

[34] Le BD, Dau F, Charles JL, Iordanoff I. Modeling damages and cracks growth in composite with a 3D discrete element method. Compos B Eng 2016;91:615–30. https://doi.org/10.1016/j.compositesb.2016.01.021.

[35] Gao W, Liu L, Liao Z, Chen S, Zang M, Tan Y. Discrete element analysis of the particle mixing performance in a ribbon mixer with a double U-shaped vessel. Granul Matter 2019;21(1):12. https://doi.org/10.1007/s10035-018-0864-4.

[36] Itasca Consulting Group Inc. PFC — particle flow code, ver. 6.0. 2019. Minneapolis: Itasca.

[37] Tanaka K, Nishida M, Kunimochi T, Takagi T. Discrete element simulation and experiment for dynamic response of two-dimensional granular matter to the impact of a spherical projectile. Powder Technol 2002;124(1):160–73. https://doi.org/10.1016/S0032-5910(01)00489-2.

[38] Shi DD, Cao D, Deng YB, Xue JF. DEM investigations of the effects of intermediate principal stress ratio and particle breakage on the critical state behaviors of granular soils. Powder Technol 2021;379:547–59. https://doi.org/10.1016/j.powtec.2020.10.094.

[39] Wang X-e, Yang J, Liu Q-f, Zhang Y-m, Zhao C. A comparative study of numerical modelling techniques for the fracture of brittle materials with specific reference to glass. Eng Struct 2017;152:493–505. https://doi.org/10.1016/j.engstruct.2017.08.050.

[40] Lu Q, Zhou S, Tao F, Luo J, Wang Z. Enhancing gene expression programming based on space partition and jump for symbolic regression. Inf Sci 2021;547:553–67. https://doi.org/10.1016/j.ins.2020.08.061.

[41] Ozbek A, Unsal M, Dikec A. Estimating uniaxial compressive strength of rocks using genetic expression programming. J Rock Mech Geotech Eng 2013;5(4):325–9. https://doi.org/10.1016/j.jrmge.2013.05.006.

[42] De Simone M, Souza LMS, Roehl D. Estimating DEM microparameters for uniaxial compression simulation with genetic programming. Int J Rock Mech Min Sci 2019;118:33–41. https://doi.org/10.1016/j.ijrmms.2019.03.024.

[43] Liu Y, Gu Z, Hughes DJ, Ye J, Hou X. Understanding mixed mode ratio of adhesively bonded joints using genetic programming (GP). Compos Struct 2021;258:113389. https://doi.org/10.1016/j.compstruct.2020.113389.

[44] Gu Z, Liu Y, Hughes DJ, Ye J, Hou X. A parametric study of adhesive bonded joints with composite material using black-box and grey-box machine learning methods: deep neuron networks and genetic programming. Compos B Eng 2021:108894. https://doi.org/10.1016/j.compositesb.2021.108894.

[45] Ferreira C. Gene expression programming: mathematical modeling by an artificial intelligence. Springer; 2006.

[46] International Organization for Standardization. ISO 527-2 Plastics — determination of tensile properties — Part 2: test conditions for moulding and extrusion plastics. 2012. Geneva.

[47] Ismail Y, Sheng Y, Yang D, Ye J. Discrete element modelling of unidirectional fibre-reinforced polymers under transverse tension. Compos B Eng 2015;73:118–25. https://doi.org/10.1016/j.compositesb.2014.12.024.

[48] Hell S, Weißgraeber P, Felger J, Becker W. A coupled stress and energy criterion for the assessment of crack initiation in single lap joints: a numerical approach. Eng Fract Mech 2014;117:112–26. https://doi.org/10.1016/j.engfracmech.2014.01.012.

[49] Kanani AY. Development of novel multi-material adhesive joints. Lancaster: Lancaster University; 2021.